An Effective Method for Detecting Dental Diseases by using Fast Neural Networks

HAZEM M. EL-BAKRY

Faculty of Computer Science & Information Systems,
Mansoura University, EGYPT
E-mail: helbakry20@yahoo.com

NIKOS MASTORAKIS

Department of Computer Science,
Military Institutions of University Education (MIUE) -
Hellenic Naval Academy, Greece

Abstract – In this paper, a new fast algorithm for dental diseases detection is presented. Such algorithm relies on performing cross correlation in the frequency domain between input image and the input weights of fast neural networks (FNNs). It is proved mathematically and practically that the number of computation steps required for the presented FNNs is less than that needed by conventional neural networks (CNNs). Simulation results using MATLAB confirm the theoretical computations. One of the limitations of Direct Digital Radiography (DDR) is noise. Some recent publications have indicated that Digital Subtraction Radiography (DSR) might significantly aid in the clinical diagnosis of dental diseases, once various clinical logistic problems limiting its widespread use have been over come. Noise in digital radiography may result from sources other than variation in projection geometry during exposure. Structure noise consists of all anatomic features other than those of diagnostic interest. Limitations of plain radiographs in detecting early, small bone lesions are also due to the presence of structure noise. This research work has been under - taken in an attempt to minimize structure noise in digital dental radiography by using digital subtraction radiography. By minimizing the structure noise, the validity of the digitized image in detecting diseases is enhanced.

Keywords— Direct digital radiography, structure noise, dental bone lesions, digital subtraction radiography, fast neural networks, cross correlation.

I. Introduction

The dental radiographic image [1] is an essential appliance for the diagnosis of periapical bone lesions. These are pathological processes situated at or surrounding the apex of a tooth accompanied with local resorption of bone. Detection and interpretation of the radiographic features leading to a diagnosis is carried out by human observers. Because this introduces subjectivity in the results, a high degree of variability might be expected. Several investigations have not only confirmed this interobserver variability, but also revealed the intraobserver variability. This means that an observer does not always draw the same conclusions at different occasions [2-5].

The aim of this research is to develop a computer aided detection technique for periapical bone lesions. The purpose of computerizing the procedure is to make maximum use of the radiologic features, to objectify detection process, and ultimately to enable bone lesions to be assessed quantitatively. It described an application of digital image analysis for the description of periapical bone lesion in dental radiography. These techniques enable the problem of observer variability to be circumvented, and can eventually be used for the quantitative assessment of bone lesions [8-11]. Since periapical bone lesions appear radiographically as dark are as compared with their surrounding tissues, an edge-detection method is developed to extract the boundaries between anatomy and pathology. The original data are transformed in such a way that only the outlines remained. The lesion is assumed by a continuous outline, so all the contour points not being part of a continuous outline are excluded. With only limited operator interaction, the lesion contour could be projected successfully onto the original image. The result of this operation is a simplified diagnostic examination process promising a higher degree of objectivity in periapical bone lesion detection. It is concluded that the results encourage further development of image processing techniques suitable for the definitive detection and diagnosis of periapical bone lesions [12-15]. We are tried by image processing and matlab program to calculate a first derivative of the next equations, denoted the derivative image and by using this method, we could remove structure noise in original image. Description of technical method and implementation of derivative formulation are shown respectively later.

II. Materials and Methods

Since improvement of overall image quality would automatically help to detect specific structures [1], in this study two assumptions are made: 1) a periapical bone lesion is considered dark in relation to its surroundings, 2) the outline of a periapical bone lesion is a closed contour. These assumptions imply a search for edges, in this case defined as boundaries

between two regions with different mean gray levels. Usually we have to deal with smooth changes in gray level, with different kinds of noise superimposed.

Edge detection is carried out by calculating a derivative function in eight directions [6] , [7]. Considering g (i, j) as the original data, the convolution function to calculate a first derivative is given by :

$$g'(i,j) = \max \left[\left| \sum_{m=0}^{1} \sum_{n=-2m}^{2m} g(i+2n, j-2m-2) - g(i+2n, j+2m+2) \right| , \left| \sum_{m=0}^{1} \sum_{n=-2m}^{2m} g(i-2m-2, j+2n) - g(i+2m+2, j+2n)) \right| , \left| \sum_{n=0}^{2} \sum_{m=2-n}^{2} (g(i-2n, j-2m) - g(i+2n, j+2m)) \right| , \left| \sum_{n=0}^{2} \sum_{m=2-n}^{2} (g(i-2n, j+2m) - g(i+2n, j-2m)) \right| \right] \quad (1)$$

Where g (i , j) denotes the original image and g' (i , j) the derivative image; i and j are pixel coordinates in a rectangular coordinate system.

This procedure resulted in high values (bright pixels) for regions with great gray level changes, and low values (dark pixels) for more homogeneous regions. Next the picture is segmented into a binary image. The chosen threshold (T) is the mean gray level of the processed image (2):

$$T = \text{int}\left[\frac{\sum g'(i,j)}{256^2} + 0.5 \right] \quad (2)$$

The result of this operation is a binary image which shows a pattern roughly resembling the contour of the bone lesion being sought. When the contour of the presumed lesion is not continuous, the operator is required to indicate two points in the bright area, one on each side of a gap in the lesion contour, after which the gap is closed by finding a path of maximum values between those two points.

For testing the procedure, different endodontic radiographs with visible periapical bone lesions are selected. They are analyzed as described above, and the results are judged by comparison with direct observation of the original image. To test the reproducibility, a single image is analyzed many times, subsequently introducing three variables:

1. Repeated analysis of the same digitize image,

2. Repeated digitization and analysis with repositioning, and

3. Repeated digitization and analysis with repositioning. Repositioning is done by taking the radiograph from light box, and putting it back again in place in a reproducible way.

Because the relationship between gray level changes due to anatomical structures and due to pathological structures is not always favorable, the outline of the lesion contour is not always continuous. Although the remaining gaps usually are not very big, more specific features for distinguishing periapical lesions could reduce the problem, and with that the role of the operator will be reduced too. Further research should aim at this subject. Considering the results of the repeated analysis of a single radiograph, the main influencing variables are the effect of operator interaction, and the inherent characteristics resulting from the imaging system. Although the influence of the operator is small already, the detection method should reduce this influence to a minimum. It is concluded that the procedure may provide a more quantitative and reproducible assessment of periapical lesions than conventional interpretation of radiographs. Radiographic information can be used more effectively, while inter- and intraexaminer variability can be reduced.

Further investigations will focus on :

1- The development of methods of image processing which encompass the relationship between volume and area, as well as the relationship between radiographic and real extent of periapical lesions, and

2- The sensitivity and specificity of the procedure when applied to clinical radiographs, compared with observers.

III. Enhancing Dental Image by Computing its Derivative

The derivative of the original image is resulted in high values (bright pixels) for regions with great gray level changes, and low values (dark pixels) for more homogeneous regions. The structure noise region in original image has a great gray level (bright pixels), after derivative original image, the bright pixels become dark pixels, therefore the structure noise is removed.

Edge detection [6] is an important problem in recognition of objects in images. When the edge detector is applied to an image, a picture is obtained consisting of edge points. Several general operations can be performed on this edge picture such as thinning of edges, tracing edge segments, joining edges, and so on. Algorithms are given that perform those operations. To show the power of the edge detector, an experiment is described in which rib boundaries are extracted in chest X-ray photographs.

A new edge detection system [7] is described, which is suitable for combining the detection and coding of visually significant edges in natural images. The

edges are defined as amplitude discontinuities between different regions of an image. The edges are defined as amplitude discontinuities between different regions of an image. The edge detection system makes use of 3 x 3 compass gradient masks, which are well suited for digital implementation. Edge angles are quantized to eight equally spaced directions, suitable for chain coding of contours. Use of an edge direction map improves the simple thresholding of gradient modulus images.

The concept of local connectivity of the edge direction map is useful in improving the performance of this method as well as other edge operators such as Kirsch and Sobel. The concepts of an "edge activity index" and a "locally adaptive threshold" an introduced and shown to improve the performance even further. In recent years, computed radiography (CR), which provides direct digital acquisition of X-ray images, has been developed and widely accepted. Conventional radiographs have had problems in image data production and transfer, but a CR technique has resolved some of these limitations, although image quality apparently is inferior to that of conventional radiographs.[8-15].

Digital subtraction radiography scheme established for aligning clinical in vivo radiographs based on the implementations of an automatic geometric registration method and a contrast correction technique [16-18]. Matrix inversion tomosynthesis (MITS) uses linear systems theory, along with a priori knowledge of the imaging geometry, to deterministically distinguish between true structure and overlying tomographic blur in a set of conventional tomosynthesis planes[19,20]. Cone beam computed tomography (CBCT), which provides a lower dose, lower cost alternative to conventional CT, is being used with increasing frequency in the practice of oral and maxillofacial radiology [21].

Matlab program is used to verify every term and to indicate the maximum of all terms in Eq. 1 and the threshold chosen (T) in Eq. 2. After inserting the original image shown in Fig. 1 in the Matlab program, the final image shown Fig. 3 after derivative became a very clear image, and rendered edge detection of the lesion more sharp because structure noise is removed. Fig. 2 and Fig. 4 show histogram of original image and the final image respectively intensity of gray level at (x) axis and number of pixels at (y) axis.

IV. Fast Dental Diseases Detection by using Neural Networks and Cross Correlation in the Frequency Domain

First neural networks are trained to classify sub-images which contain diseases from those which do not and this is done in the spatial domain. In the test phase, each sub-image in the input image (under test) is tested for the presence or absence of diseases. At each pixel position in the input image each sub-image is multiplied by a window of weights, which has the same size as the sub-image. This multiplication is done in the spatial domain. The outputs of neurons in the hidden layer are multiplied by the weights of the output layer. When the final output is high this means that the sub-image under test contain diseases and vice versa. Thus, we may conclude that this searching problem is cross correlation in the spatial domain between the image under test and the input weights of neural networks.

In this section, a fast algorithm for detecting diseases based on two dimensional cross correlations that take place between the tested image and the sliding window (20x20 pixels) is described. Such window is represented by the neural network weights situated between the input unit and the hidden layer. The convolution theorem in mathematical analysis says that a convolution of f with h is identical to the result of the following steps: let F and H be the results of the Fourier transformation of f and h in the frequency domain. Multiply F and H in the frequency domain point by point and then transform this product into spatial domain via the inverse Fourier transform [22,24]. As a result, these cross correlations can be represented by a product in the frequency domain. Thus, by using cross correlation in the frequency domain a speed up in an order of magnitude can be achieved during the detection process [22].

In the detection phase, a sub-image X of size mxz (sliding window) is extracted from the tested image, which has a size PxT, and fed to the neural network. Let W_i be the vector of weights between the input sub-image and the hidden layer. This vector has a size of mxz and can be represented as mxz matrix. The output of hidden neurons h_i can be calculated as follows:

$$h_i = g\left(\sum_{j=1}^{m} \sum_{k=1}^{z} W_i(j,k) X(j,k) + b_i \right) \qquad (3)$$

where g is the activation function and b_i is the bias of each hidden neuron *(i).* Eq. 3 represents the output of each hidden neuron for a particular sub-image I. It can be computed for the whole image Ψ as follows:

$$h_i(u,v) = g\left(\sum_{j=-m/2}^{m/2} \sum_{k=-z/2}^{z/2} W_i(j,k) \Psi(u+j, v+k) + b_i \right) \qquad (4)$$

Eq.(4) represents a cross correlation operation. Given any two functions f and g, their cross correlation can be obtained by [24]:

$$g(x,y)\otimes f(x,y)= \left(\sum_{m=-\infty}^{\infty} \sum_{z=-\infty}^{\infty} g(m,z) f(x+m,y+z) \right) \quad (5)$$

Therefore, Eq.(4) can be written as follows [22]:

$$h_i = g\left(W_i \otimes \Psi + b_i\right) \quad (6)$$

where h_i is the output of the hidden neuron *(i)* and h_i *(u,v)* is the activity of the hidden unit *(i)* when the sliding window is located at position *(u,v)* in the input image Ψ and $(u,v) \in [P-m+1, T-n+1]$.
Now, the above cross correlation can be expressed in terms of the Fourier Transform:

$$W_i \otimes \Psi = F^{-1}\left(F(\Psi) \bullet F^*\left(W_i\right)\right) \quad (7)$$

(*) means the conjugate of the *FFT* for the weight matrix. Hence, by evaluating this cross correlation, a speed up ratio can be obtained comparable to conventional neural networks. Also, the final output of the neural network can be evaluated as follows:

$$O(u,v) = g\left(\sum_{i=1}^{q} W_o(i)\, h_i(u,v) + b_o \right) \quad (8)$$

where q is the number of neurons in the hidden layer. $O(u,v)$ is the output of the neural network when the sliding window located at the position (u,v) in the input image Ψ. W_o is the weight matrix between hidden and output layer.

The complexity of cross correlation in the frequency domain can be analyzed as follows:

1. For a tested image of *NxN* pixels, the *2D-FFT* requires a number equal to $N^2 log_2 N^2$ of complex computation steps. Also, the same number of complex computation steps is required for computing the *2D-FFT* of the weight matrix for each neuron in the hidden layer.

2. At each neuron in the hidden layer, the inverse *2D-FFT* is computed. So, q backward and $(1+q)$ forward transforms have to be computed. Therefore, for an image under test, the total number of the *2D-FFT* to compute is $(2q+1)N^2 log_2 N^2$.

3. The input image and the weights should be multiplied in the frequency domain. Therefore, a number of complex computation steps equal to qN^2 should be added.

4. The number of computation steps required by the fast neural networks is complex and must be converted into a real version. It is known that the two dimensional Fast Fourier Transform requires $(N^2/2) log_2 N^2$ complex multiplications and $N^2 log_2 N^2$ complex additions [23]. Every complex multiplication is realized by six real floating point operations and every complex addition is implemented by two real floating point operations. So, the total number of computation steps required to obtain the *2D-FFT* of an *NxN* image is:

$$\rho = 6((N^2/2) log_2 N^2) + 2(N^2 log_2 N^2) \quad (9)$$

which may be simplified to:

$$\rho = 5N^2 log_2 N^2 \quad (10)$$

Performing complex dot product in the frequency domain also requires $6qN^2$ real operations.

5. In order to perform cross correlation in the frequency domain, the weight matrix must have the same size as the input image. Assume that the input object has a size of (nxn) dimensions. So, the search process will be done over sub-images of (nxn) dimensions and the weight matrix will have the same size. Therefore, a number of zeros = (N^2-n^2) must be added to the weight matrix. This requires a total real number of computation steps = $q(N^2-n^2)$ for all neurons. Moreover, after computing the *2D-FFT* for the weight matrix, the conjugate of this matrix must be obtained. So, a real number of computation steps $=qN^2$ should be added in order to obtain the conjugate of the weight matrix for all neurons. Also, a number of real computation steps equal to N is required to create butterflies complex numbers $(e^{-jk(2\Pi n/N)})$, where $0<K<L$. These $(N/2)$ complex numbers are multiplied by the elements of the input image or by previous complex numbers during the computation of the *2D-FFT*. To create a complex number requires two real floating point operations. So, the total number of computation steps required for the fast neural networks becomes:

$$\sigma = (2q+1)(5N^2 log_2 N^2) + 6qN^2 + q(N^2-n^2) + qN^2 + N \quad (10)$$

which can be reformulated as:

$$\sigma = (2q+1)(5N^2 log_2 N^2) + q(8N^2-n^2) + N \quad (12)$$

6. Using a sliding window of size nxn for the same image of *NxN* pixels, $q(2n^2-1)(N-n+1)^2$ computation steps are required when using traditional neural networks for object detection process. The theoretical speed up factor η can be evaluated as follows:

$$\eta = \frac{q(2n^2-1)(N-n+1)^2}{(2q+1)(5N^2 log_2 N^2) + q(8N^2-n^2) + N} \quad (13)$$

The theoretical speed up ratio Eq. 12 with different sizes of the input image and different in size weight matrices is listed in Table 1. Practical speed up ratio for manipulating images of different sizes and different in size weight matrices is listed in Table 2 using 2.7 GHz processor and *MATLAB ver 5.3*. An interesting property with FNNs is that the number of computation steps does not depend on either the size of the input sub-image or the size of the weight matrix (n). The effect of (n) on the number of

computation steps is very small and can be ignored. This is in contrast to CNNs in which the number of computation steps is increased with the size of both the input sub-image and the weight matrix (n).

V. Conclusion

A new fast algorithm for dental diseases detection has been presented. This has been achieved by performing cross correlation in the frequency domain between input image and the input weights of fast neural networks (FNNs). It has been proved mathematically and practically that the number of computation steps required for the presented FNNs is less than that needed by conventional neural networks (CNNs). Simulation results using MATLAB has confirmed the theoretical computations. In addition, it has been shown that after removing structure noise, digital radiographs increased diagnostic accuracy over digital radiography with structure noise. Removing structure noise offered a superb method of diagnosing periapical lesions affecting dental structures and clearly demonstrated any effects on the teeth and surrounding vital structures. The human errors inherent with visual interpretation of dental diseases from images will be minimum due to increasing the image characteristics after noise removal. This is a step forward in achieving accurate diagnosis as well as increasing the utility of digitized radiographs in providing qualitative and quantitative information concerning the investigated diseases.

References

[1] Mol, A., Paul F., and Stelt, VD., ‘‘Application of digital image analysis in dental radiography for the description of periapical bone lesions: A preliminary study’’, IEEE Transactions on Biomedical Engineering, vol. 38, No. 4, April 1991, pp. 357-359.

[2] Moyen, F., Benz, c., Sonnabend, E., and Lodter, J.P., ‘‘Presentation and physical evaluation of radiovisiography’’, Oral Surg Oral Med Oral Pathol, vol. 68, 1989, pp. 238-242.

[3] Allan, GF., ‘‘Basic technical properties of a system for direct acquisition of digital intraoral radiographs’’, Oral Surg Oral Med Oral Pathol, vol. 75, 1993, pp. 506-511.

[4] Reddy, MS., Bruch, JM., Jeffcoat, MK., and Williams, RC., **‘‘**Contrast enhancement as an aid to interpretation in digital subtraction radiography**’’,** Oral Surg Oral Med Oral Pathol, vol.71, 1991, pp. 763-769.

[5] Wenzal, A., ‘‘Sensor noise indirect digital imaging (the radiovisiography, Sens-A-Ray and Visualix/Vixa systems) evaluated by subtraction radiography’’, Oral Surge Oral Med Oral Pathol, vol.77, 1994, pp. 70-74.

[6] Persoon, E., ‘‘A new edge detection algorithm and its applications in Picture processing’’, Computer Graphics and Image Processing, vol. 5, 1986, pp. 425-446.

[7] Robinson, GS., ‘‘Edge detection by compass gradient masks’’, Computer Graphics and Image processing, vol. 6, 1987, pp. 492-501.

[8] Chen, S-K., and Hollender, L., ‘‘Detector response and exposure control of the radiovisiography system (RVG 32000 ZHR)’’, Oral Surg Oral Med Oral Pathol, vol. 76, 1993, pp. 104-111.

[9] Hormer, k.,Shearer, AC., Walker, A., and Wilson, NHF., ‘‘Radiovisiography: an initial evaluation’’, Britch Dental Journal, vol. 168 , 1990, pp. 244-248.

[10] Benz, C., and Mouyen, F., ‘‘Evaluation of the new Radio VisioGraphy system image quality’’, Oral Surg Oral Med Oral Pathole, vol.72, 1991, pp. 627-631.

[11] Nelvig, p., Wing, k., and Welander, u., **‘‘**Sens-A-Ray a new system for direct digital intraoral radiography’’, Oral Surg Oral Med Oral Pathol, vol .74, 1992, pp. 818-832.

[12] Gonzalo, RA., **‘‘**A General weighted Median Filter Structure Admitting Negative weights’’, IEEE Transactions on signal processing, vol. 46, No.12, December 1998, pp. 3195-3205.

[13] Philip S., ‘‘Size-Sensitive multire solution decomposition of images with rank order based filters’’, Signal processing, vol. 27, 1992, pp. 205-241.

[14] Lehman, TM., Troeltsch, E., and Spitzer, k., ‘‘Image processing and enhancement provided by commercial dental software programs’’, Dentomaxillofacial Radiolgy, vol. 31, 2002, pp. 264-272.

[15] Chum-shien Lu., and Hong-Yuan ML., ‘‘Structural digital signature for image Authentication: An Incidental Distortion Resistant scheme’’, IEEE Transactions on Multimedia, vol. 5, No.2, June 2003.

[16] Nakagawa, K., Mizuno, S., Aoki, Y., and Ohtomo, K., ‘‘C-MOS Flat-panel sensor for real-time X-ray imaging’’, Radiation Medicine, vol. 18, No. 6, 2000, pp. 349-354.

[17] Zacharaki, EI., Matsopoulos, GK., Asvestas, PA., Nkita, KS., Grondahl, K., and Grondahl, H-G., ‘‘A digital subtraction radiography secheme based on automatic multiresoluion registration’’, Dentomaxillofacial Radiology, Vol. 33, 2004, pp. 379-390.

[18] Akdeniz, BG., Sogur, E., **‘‘**An ex vivo comparison of conventional and digital radiography for perceived image quality of root fillings’’, International Endodontic Journal. vol. 38, 2000, pp. 397-401.

[19] Godfrey, DJ., McAdams, HP.; and Dobbins, JT., ‘‘Optimization of the matrix inversion tomosynthesis (MITS) impulse response and modulation transfer function characteristics for chest imaging’’, Medical Physics, vol. 33, 2006, pp. 655-667.
[20] Ludlow, JB., Davies-Ludlow, LE., Brooks, SL., and Howerton, WB., ‘‘Dosimetry of 3 CBCT devices for oral and maxillofacial radiology: CB Mercuray, New Tom 3G and i-CAT’’, Dentomaxillo facial Radiology, Vol. 35, pp. 219-226, (2006).
[21] Anis Ebrahim, N. M., Minimizing Structure Noise In Digital Dental Radiography, Phd Thesis, Cairo university, Egypt, 2008.
[22] El-Bakry, H. M., "New Faster Normalized Neural Networks for Sub-Matrix Detection using Cross Correlation in the Frequency Domain and Matrix Decomposition," Applied Soft Computing journal, vol. 8, issue 2, March 2008, pp. 1131-1149.
[23] Cooley, J. W. and Tukey, J. W., "An algorithm for the machine calculation of complex Fourier series," Math. Comput. 19, 1965, pp. 297–301.
[24] Klette R., and Zamperon, "Handbook of image processing operators, " John Wiley & Sonsltd, 1996.
[25] El-Bakry, H. M., and Mastorakis, N., " A New Technique for Detecting Dental Diseases by using High Speed Neuro-Computers," WSEAS Trans. On Signal Processing, vol. 8, issue 2, October 2008, pp. 1131-1149.

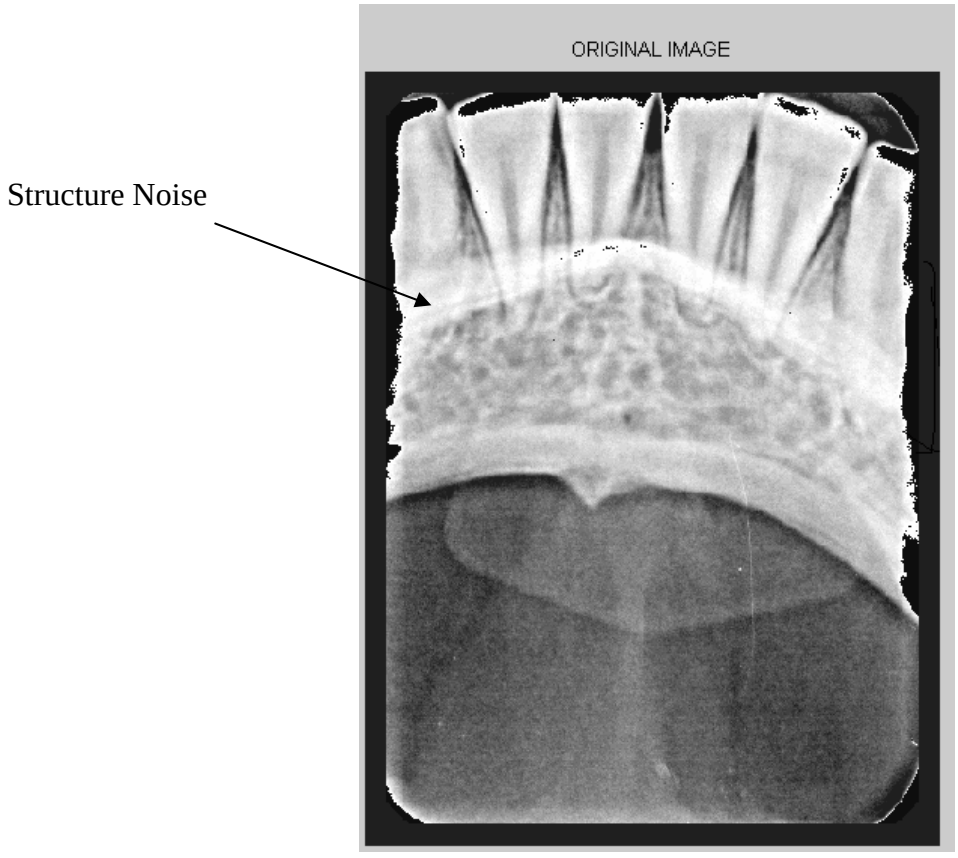

Fig. 1. Original image with structure noise.

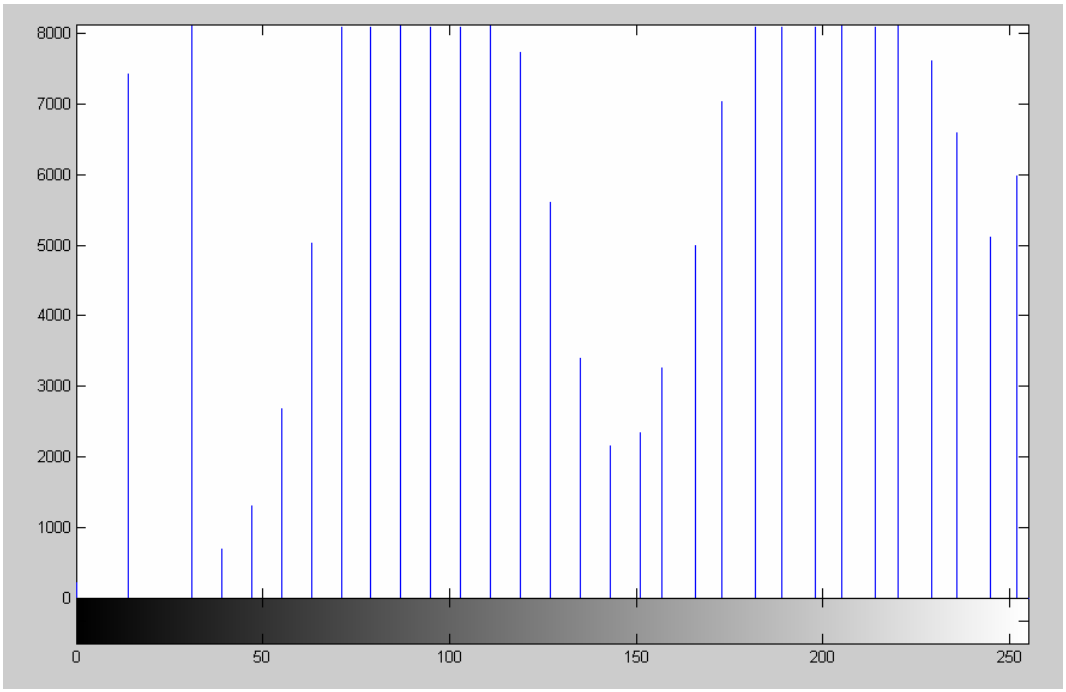

Fig. 2. Histogram of the original image.

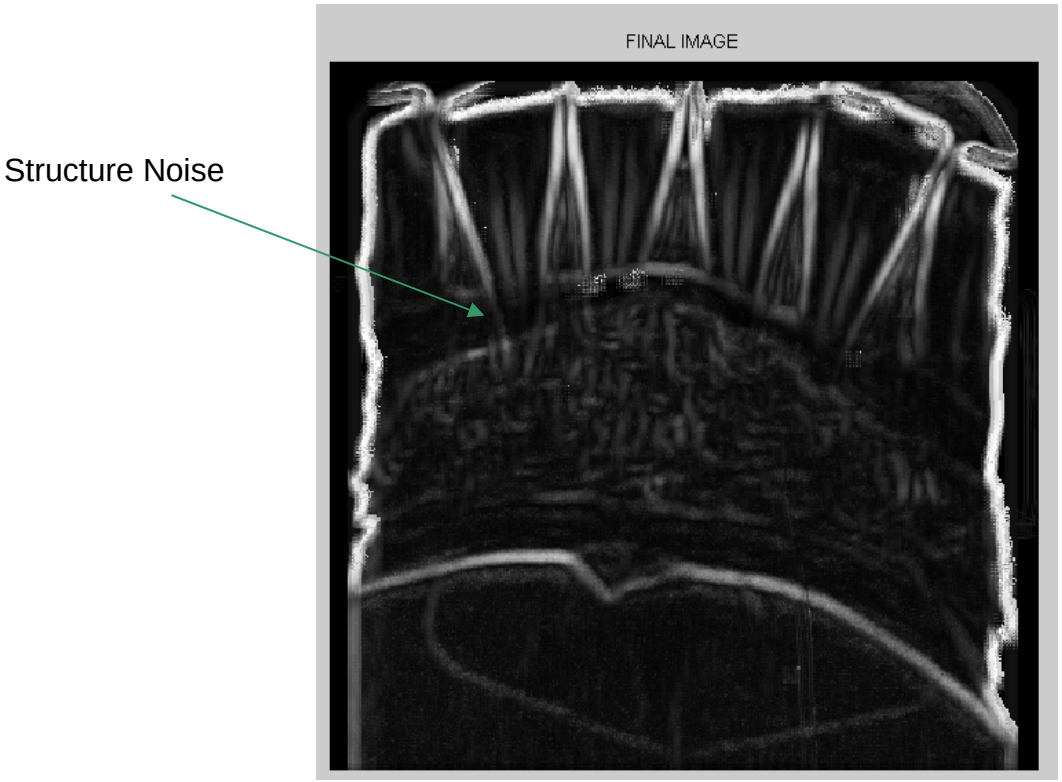

Fig. 3. Final image of original image after removing structure noise.

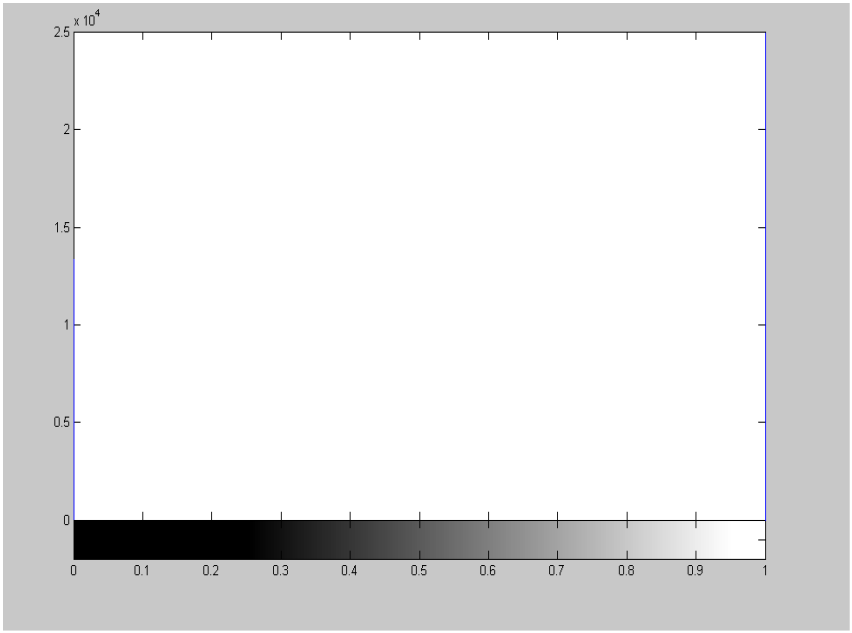

Fig. 4. Histogram of final image.

Table 1
The Theoretical Speed up Ratio for Images with Different Sizes.

Image size	Speed up ratio (n=20)	Speed up ratio (n=25)	Speed up ratio (n=30)
100x100	3.67	5.04	6.34
200x200	4.01	5.92	8.05
300x300	4.00	6.03	8.37
400x400	3.95	6.01	8.42
500x500	3.89	5.95	8.39
600x600	3.83	5.88	8.33
700x700	3.78	5.82	8.26
800x800	3.73	5.76	8.19
900x900	3.69	5.70	8.12
1000x1000	3.65	5.65	8.05
1100x1100	3.62	5.60	7.99
1200x1200	3.58	5.55	7.93
1300x1300	3.55	5.51	7.93
1400x1400	3.53	5.47	7.82
1500x1500	3.50	5.43	7.77
1600x1600	3.48	5.43	7.72
1700x1700	3.45	5.37	7.68
1800x1800	3.43	5.34	7.64
1900x1900	3.41	5.31	7.60
2000x2000	3.40	5.28	7.56

Table 2
Practical Speed up Ratio for Images with Different Sizes using MATLAB Ver 5.3.

Image size	Speed up ratio (n=20)	Speed up ratio (n=25)	Speed up ratio (n=30)
100x100	7.88	10.75	14.69
200x200	6.21	9.19	13.17
300x300	5.54	8.43	12.21
400x400	4.78	7.45	11.41
500x500	4.68	7.13	10.79
600x600	4.46	6.97	10.28
700x700	4.34	6.83	9.81
800x800	4.27	6.68	9.60
900x900	4.31	6.79	9.72
1000x1000	4.19	6.59	9.46
1100x1100	4.24	6.66	9.62
1200x1200	4.20	6.62	9.57
1300x1300	4.17	6.57	9.53
1400x1400	4.13	6.53	9.49
1500x1500	4.10	6.49	9.45
1600x1600	4.07	6.45	9.41
1700x1700	4.03	6.41	9.37
1800x1800	4.00	6.38	9.32
1900x1900	3.97	6.35	9.28
2000x2000	3.94	6.31	9.25